

Effects of dense quark matter on gluon propagators in lattice QC₂D

V. G. Bornyakov^{a,b} V. V. Braguta^{b,c,d,e} A. A. Nikolaev^f R. N. Rogalyov^a

^a*NRC "Kurchatov Institute" - IHEP, 142281 Protvino, Russia*

^b*School of Biomedicine, Far East Federal University, 690950 Vladivostok, Russia*

^c*NRC "Kurchatov Institute" - ITEP, 117259 Moscow, Russia*

^d*Bogoliubov Laboratory of Theoretical Physics, Joint Institute for Nuclear Research, Dubna, 141980 Russia*

^e*Moscow Institute of Physics and Technology, Institutsky lane 9, Dolgoprudny, Moscow region, 141700 Russia*

^f*Department of Physics, College of Science, Swansea University, Swansea SA2 8PP, United Kingdom*

E-mail: Vitaly.Bornyakov@ihep.ru, braguta@itep.ru,
aleksandr.nikolaev@swansea.ac.uk, Roman.Rogalyov@ihep.ru

ABSTRACT: The transverse and longitudinal gluon propagators in the Landau gauge are studied in the two-color lattice QCD at nonzero quark chemical potential μ_q . Parametrization of the momentum dependence of the propagators is provided for all values of chemical potential under study. We find that the longitudinal propagator is infrared suppressed at nonzero μ_q with suppression increasing with increasing μ_q . The transverse propagator dependence on μ_q was found to be opposite: it is enhanced at large μ_q . It is found, respectively, that the electric screening mass is increasing while the magnetic screening mass is decreasing with increasing μ_q . Nice agreement between the electric screening mass computed from the longitudinal propagator and the Debye mass computed earlier from the singlet static quark-antiquark potential was found. We discuss how the dependence of the propagators on the chemical potential correlates with the respective dependence of the string tension. Additionally, we consider the difference between two propagators as a function of the momentum and make interesting observations.

Contents

1	Introduction	1
2	Simulation details	3
3	Momentum dependence	5
4	Screening masses	7
5	$D_L - D_T$ as an indicator of transitions	10
6	Conclusions	12
A	Fit results	16

1 Introduction

Understanding of the phase diagram of the strong interactions is of high importance for experimental studies of hadronic matter created in relativistic heavy ion collisions. The most difficult for theoretical investigation part of this phase diagram is at low temperature and high density. The lattice QCD being the non-perturbative first principles approach very successful at zero baryon density is inapplicable at large baryon density due to the so-called sign problem [1]. This makes important to study the models similar to QCD (QCD-like) but without sign problem. In particular, two popular QCD-like theories are QCD with $SU(2)$ gauge group [2] (to be called below QC₂D) and QCD with nonzero isospin chemical potential [3]. QCD with the isospin chemical potential was intensively studied both within lattice and theoretical approaches (see, for instance, [3–8]). In this paper we are going to focus on QC₂D at nonzero quark chemical potential μ_q . Although a two-color QCD differs from the three-color QCD, lattice study of QC₂D at nonzero quark chemical potential can provide us with important information about the properties of QCD with non-zero baryon density.

QC₂D was studied using various approaches: chiral perturbation theory [2, 9, 10], Nambu-Jona-Lasinio model [11–13], quark-meson-diquark model [14, 15], random matrix theory [16, 17], Dyson-Schwinger equations [18], massive perturbation theory [19, 20]. These studies suggested the following phase structure of low-temperature QC₂D. There is a hadronic phase at $\mu_q < \mu_c = \mu_\pi/2$, Bose-Einstein condensation phase at $\mu_c < \mu_q < \mu_d$, and the phase with diquark condensation due to the Bardeen-Cooper-Schrieffer mechanism at $\mu_q > \mu_d$.

It is worth to note that these approaches are also applicable to QCD at high baryon density. It is thus useful to check them in the case of QC₂D confronting respective results with first principles lattice results.

Lattice studies of QC₂D were undertaken with both staggered fermions [21–28] for $N_f = 4$ or, more recently, $N_f = 2$ and Wilson fermions [29–35] for $N_f = 2$ mostly. In general the lattice results supported the phase structure described above.

The question of the confinement-deconfinement transition in QC₂D at low temperature is still under debate. In our recent paper [26] we studied $N_f = 2$ lattice QC₂D with staggered fermionic action at large quark density and $T = 0$ and demonstrated that the string tension σ decreases with increasing μ_q and becomes compatible with zero for μ_q above 850 MeV. The simulations were carried out at small lattice spacing $a = 0.044$ fm which was few times smaller than in all other lattice studies. This allowed to reach the range of large quark chemical potential avoiding strong lattice artifacts. In a more recent paper [36] where $N_f = 2$ lattice QC₂D with Wilson fermionic action was studied the authors did not find the confinement-deconfinement transition at low temperature. It is worth to note that in [36] rather coarse lattices were used with lattice spacings three times or more larger than in our study [26]. Thus the range of large μ_q where we found the transition to deconfinement was reached in [36] at parameter $a\mu_q > 0.5$ implying possibility of strong lattice artifacts.

In this paper we concentrate on the study of the Landau gauge gluon propagators in $N_f = 2$ lattice QC₂D at zero temperature and varying quark chemical potential. We use the same lattice action as in [26, 27] and in fact the same set of the lattice configurations. Our goal is to study how the gluon propagators change when QC₂D goes through its transitions mentioned above: from hadron phase to superfluid phase, confinement-deconfinement transition, disappearance of the spatial string tension. Some results of our study of gluon propagators were presented in [37]. Here we extend the range of μ_q values, make more detailed comparison of two definitions of the screening masses and consider in more detail the momentum dependence of the gluon propagators. We also study new observable, the difference between the (color-)electric and magnetic propagators and study its dependence on the momentum and quark chemical potential.

The gluon propagators are among important quantities to study, e.g. they play crucial role in the Dyson-Schwinger equations approach. Landau gauge gluon propagators in non-Abelian gauge theories at zero and nonzero temperature were extensively studied in the infrared range of momenta by various methods. We shall note lattice gauge theory, Dyson-Schwinger equations, Gribov-Zwanziger approach. At the same time the studies in the particular case of nonzero quark chemical potential are restricted to a few papers only. For the lattice QCD this is explained by the sign problem mentioned above.

The gluon propagators in lattice QC₂D at zero and nonzero μ_q were studied for the first time in [30]. This study was continued in [34, 38, 39]. The main conclusion of Ref. [34] was that the gluon propagators practically do not change for the range $\mu_q < 1.1$ GeV. Our main conclusion is opposite. We found substantial influence of the quark chemical potential on the gluon propagators starting from rather low values ($\mu_q \sim 300$ MeV) and increasing with increasing μ_q . Part of our results were presented in [37]. The gluon propagators

in QC₂D at nonzero μ_q were also studied in Ref. [18] with help of the Dyson-Schwinger equations approach and in Ref. [20] using the massive Yang-Mills theory approach at one-loop. The authors emphasize that after the agreement with the lattice results for the gluon propagators will be reached their methods could be applied to real QCD at nonzero baryon density. Thus to provide unbiased lattice results is very important.

The paper is organized as follows. In Section 2 we specify details of the lattice setup to be used: lattice action, definition of the propagators and details of the simulation. In the next Section we present the numerical results for the momentum dependence of the propagators and our fits to the data. Section 4 is devoted to the screening masses computation and study of their dependence on the chemical potential. In Section 5 results for the difference between the longitudinal and the transverse propagators are presented. The last section is devoted to the discussion of the results and to conclusions to be drawn.

2 Simulation details

We carry out our study using 32^4 lattices for a set of the chemical potentials in the range $a\mu_q \in (0, 0.5)$. The tree level improved Symanzik gauge action [40] and the staggered fermion action with a diquark source term [21] were used. The lattice configurations were generated at a small value of the diquark source term coupling $\lambda = 0.00075$ which was much smaller than the quark mass in lattice units $am_q = 0.0075$. More details on the generation of these lattice configurations can be found in Ref. [26]. The pion mass for this ensemble is rather large, $m_\pi/\sqrt{\sigma} = 1.56(8)$. In this paper we prefer to use the dimensionless quantities of the type m^2/σ using the value $\sqrt{\sigma}a = 0.106(1)$ [26] for this purpose. In case we use the physical units the value for the Sommer scale $r_0 = 0.468(4)$ fm [41] and relation $r_0/a = 10.6(2)$ [26] are used to convert the lattice spacing a into physical units.

To reach large quark densities without lattice artifacts one needs sufficiently small lattice spacing to satisfy condition $a\mu_q \ll 1$. At the same time to study the gluon propagators in the infrared region it is necessary to employ large physical volume. As a result of a compromise between these two requirements our lattice size is rather moderate : $L = 3.4/\sqrt{\sigma} = 1.4$ fm. This implies a potential problem of large finite volume effects at small momenta. We come to this problem again at the end of this section.

In the Introduction we briefly described the phase diagram of dense QC₂D at zero temperature. Here we want to describe this phase diagram boundaries in units of $\sqrt{\sigma}$ using results obtained in our previous papers [25–27]. For small values of the chemical potential $\mu_q < \mu_c$, where $\mu_c = m_\pi/2 \approx 0.78 \cdot \sqrt{\sigma}$, the system is in the hadronic phase. In this phase the system exhibits confinement and chiral symmetry is broken. At $\mu_q = \mu_c$ there is a second order phase transition to a phase where scalar diquarks form a Bose-Einstein condensate (BEC phase). Enhancing the baryon density further, we proceed to dense matter. At sufficiently large baryon density some observables of the system under study can be described using Bardeen-Cooper-Schrieffer theory (BCS phase). In particular, the baryon density is well described by the density of non-interacting fermions which occupy a Fermi sphere of radius $r_F = \mu_q$. The diquark condensate, which plays the role of a condensate of Cooper pairs, is proportional to the Fermi surface.

In addition to the transition to the BCS phase we found [26] the confinement - deconfinement transition at $\mu_q/\sqrt{\sigma} \sim 2.1$. This transition manifests itself in a rise of the Polyakov loop and vanishing of the string tension. It is interesting that the transition to the BEC phase and the confinement - deconfinement transition are located close to each other as show our preliminary results. It was also observed in [26] that above the deconfinement transition the spatial string tension σ_s monotonously decreases and vanishes at $\mu_q/\sqrt{\sigma} \sim 4.2$.

In our study of the gluon propagators we employ the standard definition of the lattice gauge vector potential $A_{x,\mu}$ [42]:

$$A_{x,\mu} = \frac{1}{2ia g} \left(U_{x\mu} - U_{x\mu}^\dagger \right) \equiv A_{x,\mu}^a \frac{\sigma_a}{2}. \quad (2.1)$$

The lattice Landau gauge fixing condition is

$$(\nabla^B A)_x \equiv \frac{1}{a} \sum_{\mu=1}^4 (A_{x,\mu} - A_{x-a\hat{\mu},\mu}) = 0, \quad (2.2)$$

which is equivalent to finding an extremum of the gauge functional

$$F_U(\omega) = \frac{1}{4V} \sum_{x\mu} \frac{1}{2} \text{Tr} U_{x\mu}^\omega, \quad (2.3)$$

with respect to gauge transformations ω_x . To fix the Landau gauge we use the simulated annealing (SA) algorithm with finalizing overrelaxation [43]. To estimate the Gribov copy effect, we employed five gauge copies of each configuration; however, the difference between the "best-copy" and "worst-copy" values of each quantity under consideration lies within statistical errors.

The gluon propagator $D_{\mu\nu}^{ab}(p)$ is defined as follows:

$$D_{\mu\nu}^{ab}(p) = \frac{1}{V a^4} \langle \tilde{A}_\mu^a(q) \tilde{A}_\nu^b(-q) \rangle, \quad (2.4)$$

where

$$\tilde{A}_\mu^b(q) = a^4 \sum_x A_{x,\mu}^b \exp \left(i q \left(x + \frac{\hat{\mu} a}{2} \right) \right), \quad (2.5)$$

$q_i \in (-N_s/2, N_s/2]$, $q_4 \in (-N_t/2, N_t/2]$ and the physical momenta p_μ are defined by the relations $ap_i = 2 \sin(\pi q_i/N_s)$, $ap_4 = 2 \sin(\pi q_4/N_t)$.

At nonzero μ_q the $O(4)$ symmetry is broken and there are two tensor structures for the gluon propagator [44]:

$$D_{\mu\nu}^{ab}(p) = \delta_{ab} \left(P_{\mu\nu}^T(p) D_T(p) + P_{\mu\nu}^L(p) D_L(p) \right). \quad (2.6)$$

We consider the soft modes $p_4 = 0$ and use the notation $D_{L,T}(p) = D_{L,T}(0, |\vec{p}|)$.

Next we come back to discussion of the finite volume effects. At sufficiently high density the chromoelectric screening length determined as the inverse of the chromoelectric mass is estimated in perturbation theory as follows:

$$l_E = \frac{1}{m_E} \sim \frac{1}{g(\mu_q) \mu_q}$$

Our results are in agreement with this prediction as will be demonstrated in Section 4. Thus we expect that for sufficiently large μ_q there should be no large finite volume effects for the longitudinal propagator $D_L(p)$.

The screening length associated with the transverse propagator $D_T(p)$ is defined as the inverse of the chromomagnetic screening mass m_M . Perturbation theory predicts zero value of the magnetic screening mass at high chemical potentials [45]; for this reason the nonperturbative estimates of m_M are of particular interest.

We expect that at sufficiently high chemical potentials in agreement with perturbation theory the chromomagnetic screening mass goes down, the respective screening length becomes large, and to study the infrared behavior of $D_T(p)$ large lattices are needed. It should be noticed that these arguments apply to QCD at high baryon density as well.

3 Momentum dependence

In this section we consider the momentum dependence of the gluon propagators for various values of μ_q . The propagators are renormalized according to the MOM scheme to satisfy the condition

$$D_{L,T}(p = \kappa) = 1/\kappa^2 \quad (3.1)$$

at $\kappa = 12.6\sqrt{\sigma}$.

In Figure 1(left) we present the momentum dependence for the longitudinal propagator $D_L(p)$ for seven selected values of μ_q . One can see that the infrared suppression of the propagator is clearly increasing with increasing μ_q . This infrared suppression hints on the increasing of the electric screening mass. We will study the screening mass in the next section. The increasing of the infrared suppression of $D_L(p)$ with increasing μ_q is analogous to the well established behavior of $D_L(p)$ with increasing temperature in the deconfinement phase of both gluodynamics and QCD.

In Figure 1(right) the momentum dependence for the transverse propagator $D_T(p)$ for the same values of μ_q is shown. It is clear that $D_T(p)$ is much less sensitive to changes of μ_q . We found decreasing of the respective screening mass at large μ_q as will be discussed in the next section. It is known that at a finite temperature the propagator $D_T(p)$ has a clear maximum at the value of momentum increasing with temperature. Our data give no evidence for such maximum at a small momentum, however, we cannot exclude its existence.

We would like to provide an interpolation function for our data. It was demonstrated many times [46–50] that the infrared behavior of the gluon propagators at zero and finite temperature can be well described by the fit function which is the tree level prediction of the Refined Gribov-Zwanziger approach [51].

$$D_{L,T}(p) = Z_{L,T} \frac{1 + \delta_{L,T} p^2}{p^4 + 2R_{L,T} p^2 + M_{L,T}^2} . \quad (3.2)$$

Our data for nonzero momentum start at rather large value $p_{min}/\sqrt{\sigma} = 1.85(2)$. For this reason our fit results over the infrared region might suffer from finite volumes effects. Still,

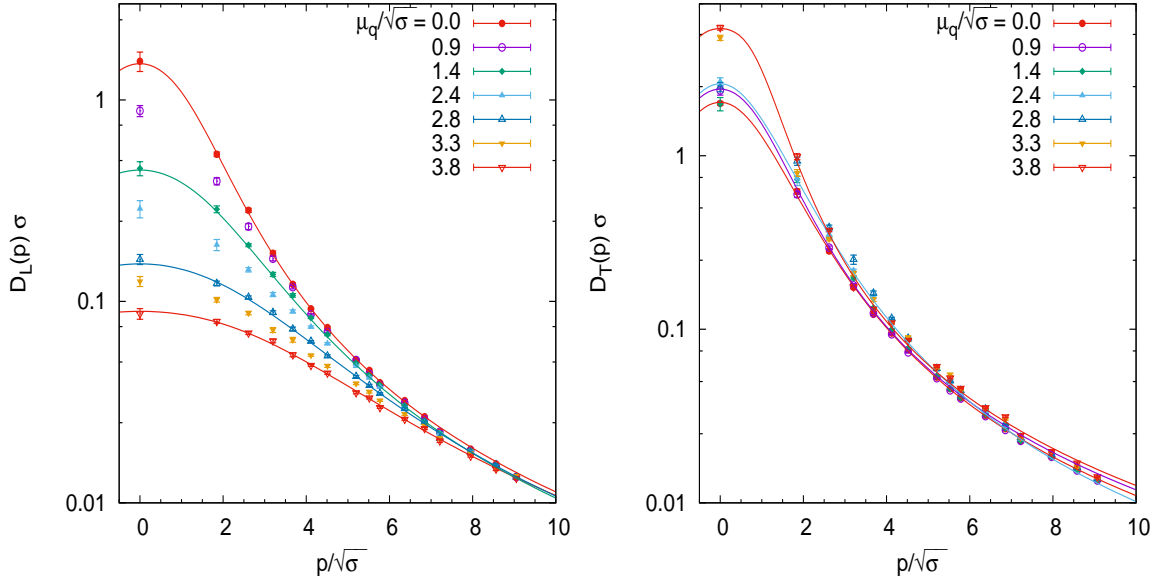


Figure 1. The propagators D_L (left) and D_T (right) as functions of p at different values of μ_q . The curves show results of the fit to eq. (3.2)

we believe that our results provide qualitatively correct dependence on μ_q , in particular for D_L at large μ_q , see relevant discussion in Section 3.

In [37] we found that the fit of the data motivated by the one loop perturbative expression works well for $p > p_{cut}$ where p_{cut} depends on μ_q for D_L . We now employ the fit (3.2) over the momentum $p < p_{cut}$. In the case of the transverse propagator $p_{cut} = 6.0 \sqrt{\sigma}$, for the longitudinal propagator p_{cut} depends on μ_q and is determined by the expression

$$p_{cut} = 3.8\sqrt{\sigma} + \mu_q. \quad (3.3)$$

An attempt to increase the fitting range beyond p_{cut} gives rise to substantial decreasing of the fit quality in most cases. It was also found that beyond this domain the perturbatively motivated fit works well [37].

The results for the fit parameters for $D_L(p)$ are presented in Appendix A, Table 1. The fits for large μ_q were not successful. Using the Table the practitioners of other approaches to QC₂D can compare their results with ours¹.

In practice we fitted the ratio $D_{L,T}(p)/D_{L,T}(p_0)$ with $p_0/\sqrt{\sigma} = 6.3$. This allowed us to decrease uncertainties in the fit parameters $M_{L,T}^2, R_{L,T}, \delta_{L,T}$. Respectively, the parameters $Z_{L,T}$ were not determined from the fitting procedure but re computed (for renormalized propagator) via relation

$$Z_{L,T} = D_{L,T}(p_0) \frac{p_0^4 + 2R_{L,T}p_0^2 + M_{L,T}^2}{1 + \delta_{L,T}p_0^2}. \quad (3.4)$$

¹We do not present correlations between the fitting parameters M, R , and δ . For this reason the error in $D_{L,T}(p)$ evaluated from the data in Tables 1 and 2 assuming zero correlations between parameters provides an overestimated error. In so doing, the error in Z can be safely neglected and we do not show it.

Results of the fits for $D_L(p)$ are also shown in the Figure 1(left) together with the lattice data. For the hadron phase the propagators do not change much with increasing μ_q . For this reason absence of a systematic dependence of the parameters on μ_q at small μ_q is not a surprise. For $D_L(p)$ the μ_q dependence of the fit parameters are similar: beyond the hadron phase M_L^2 , R_L and $1/\delta_L$ are increasing with μ_q .

In the case of the transverse propagator the fits were successful for $\mu_q/\sqrt{\sigma} < 3.0$, see Table 2. The fit parameters M_T^2 , R_T and $1/\delta_T$ again show qualitatively similar dependence on μ_q . Their values are lower at the intermediate values $1.0 < \mu_q/\sqrt{\sigma} < 1.8$ than in the hadron phase and then increase again at $\mu_q/\sqrt{\sigma} \gtrsim 1.8$ to roughly same values (M_T^2 and R_T) or to higher values ($1/\delta_T$) than in the hadron phase.

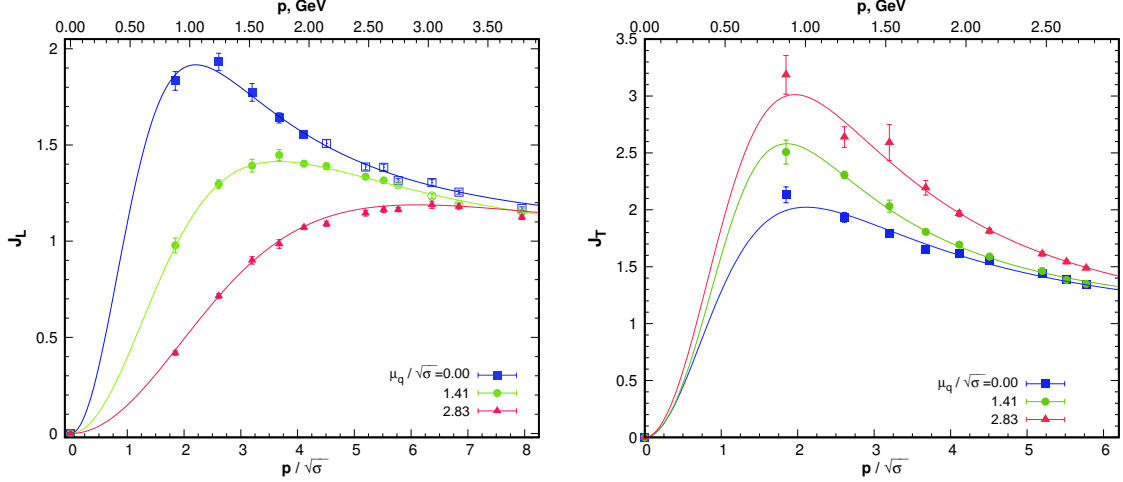


Figure 2. Dressing functions J_L and J_T as functions of p at different values of μ_q . Empty symbols in the left panel are those beyond our fitting range (3.3).

It is instructive to look also at the respective dressing functions $J_{L,T}(p)$ defined as

$$J_{L,T}(p) = p^2 D_{L,T}(p) \quad (3.5)$$

It is seen in Figure 2 (left) that with increasing μ_q the maximum of the longitudinal dressing function goes down and shifts to the right, thus approaching dressing function of a massive scalar particle. We note once more that this dependence on μ_q is very similar to dependence on the temperature, see e.g. Ref. [52].

As can be seen in Figure 2(right) the transverse dressing function shows instead infrared enhancement with increasing μ_q . This is in agreement with the disappearance of the magnetic field screening at extremely large quark chemical potential predicted in [45].

4 Screening masses

The widely used definition of the screening mass, see the review [53] and references therein, is through the inverse of the propagator at zero momentum

$$m_E^2 = \frac{1}{D_L(0)}, \quad m_M^2 = \frac{1}{D_T(0)}. \quad (4.1)$$

It is clear, that the screening mass defined by eq. (4.1) depends on renormalization. Moreover, it is rather sensitive to the finite volume effects. Loosely speaking, eq. (4.1) characterizes “the total amount” of the interaction since

$$\frac{1}{m_{E,M}^2} = \int dx_4 d\vec{x} D_{L,T}(x_4, \vec{x}), \quad (4.2)$$

where $D_{L,T}(x_4, \vec{x})$ are the propagators in the coordinate representation.

We also consider another definition of the screening mass using fitting of $D_{L,T}^{-1}(p)$ at low momenta by Taylor expansion in p^2 :

$$D_{L,T}^{-1}(p) = Z^{-1}(\tilde{m}_{E,M}^2 + p^2 + c_4 \cdot (p^2)^2 + \dots). \quad (4.3)$$

This method was used in [54] in studies of lattice QCD at finite temperature and we applied it to QC₂D in [37]. In fact it would be more consistent to use the Yukawa type fitting function

$$D_{L,T}^{-1}(p) = Z^{-1}(\tilde{m}_{E,M}^2 + p^2) \quad (4.4)$$

as was done in [55–57] in studies of lattice gluodynamics at zero and finite temperature. It was shown in [57] that the Yukawa type function (4.4) provides constant value for \tilde{m}_E^2 over rather wide range of momenta in the infrared. The reason we are using function (4.3) rather than function (4.4) is that we have not enough data points in the infrared region where the propagator can be described by the function (4.4). Thus, to obtain a reasonable fit results we had to use terms up to $(p^2)^2$ for $D_L(p)$ and terms up to $(p^2)^3$ for $D_T(p)$. Still, we hope that making use of the fit function (4.3) provides reasonably good estimates of the parameters in eq. (4.4).

Let us note that the definition of $\tilde{m}_{E,M}^2$ can be related to the definition of the correlation length:

$$\tilde{m}_{E,M}^2 = \xi_{E,M}^{-2}, \quad (4.5)$$

where the correlation length $\xi_{E,M}$ is conventionally defined in terms of the correlation function (propagator in our case) by the expression [58]

$$\xi^2 = \frac{1}{2} \frac{\int_V dx_4 d\vec{x} \tilde{D}(x_4, \vec{x}) |\vec{x}|^2}{\int_V dx_4 d\vec{x} D(x_4, \vec{x})} = -\frac{1}{2D(0, \vec{0})} \sum_{i=1}^3 \left(\frac{d}{dp_i} \right)^2 \Big|_{\vec{p}=0} D(0, \vec{p}). \quad (4.6)$$

Even after the propagators are renormalized the definitions of the screening mass (4.5–4.6) and (4.1) differ in general by a factor which may depend on the chemical potential or temperature. Its temperature dependence was found in $SU(3)$ gluodynamics [57].

In Figure 3 we show the electric (left panel) and magnetic (right panel) masses defined according to these two definitions. Our value for $\tilde{m}_E/\sqrt{\sigma}$ at $\mu_q = 0$ is 1.50(4). This value can be compared with the value 1.47(2) obtained in $SU(3)$ gluodynamics at zero temperature [56] by fitting the inverse propagator to the form (4.4) at small momenta² We also quote a value 1.48(5) obtained for a mass dominating the small momentum behavior of a gluon propagator in $SU(2)$ lattice gluodynamics in [59].

²We obtained this value taking mass value 647(7) MeV, obtained in [56] and dividing it by $\sqrt{\sigma} = 440$ MeV used in [56] to set the scale.

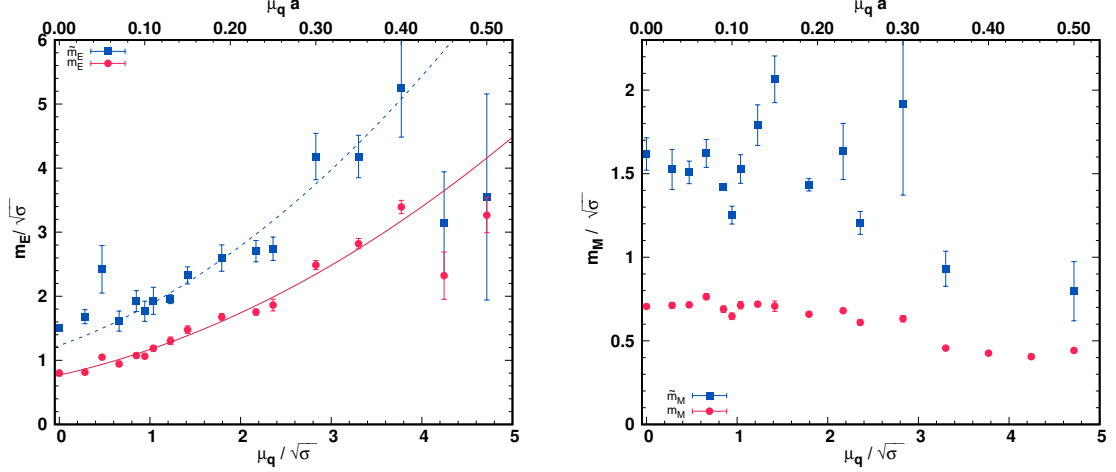


Figure 3. Electric (left panel) and magnetic (right panel) screening masses defined by eq. (4.5-4.6) (squares) and by eq. (4.1) (circles) as functions of μ_q . The curves in the left panel are described in the text.)

One can see that m_E and \tilde{m}_E show qualitatively very similar dependence on μ_q . They do not change much at small μ_q corresponding to the hadron phase. Above $\mu_q / \sqrt{\sigma} \approx 0.5$ they start to increase and continue to increase at all μ_q values. This behavior is similar to increasing of the electric screening mass with increasing temperature in QCD at $T > T_c$ as was demonstrated by lattice simulations with definition (4.1) in [52, 57, 60] and with definition (4.5-4.6) in [55, 57]. No such increasing was reported in Ref. [34].

In Ref. [37] we found that the ratio \tilde{m}_E / m_E can be well approximated by a constant 1.6 for the range $0.9 < \mu_q / \sqrt{\sigma} < 3.0$. Now we can confirm this conclusion for higher μ_q included in this paper. The lower curve in this Figure shows fit of m_E values by a polynomial of degree two. The upper curve is obtained by multiplication with factor 1.6. One can see that the upper curve agree well with \tilde{m}_E . The visible deviation is observed for the hadron phase only as we reported in Ref. [37].

From the Figure 3 (right) one can see that the magnetic screening masses m_M and \tilde{m}_M also have qualitatively similar dependence on μ_q , although with one exception: \tilde{m}_M shows increasing in the range $1.0 \lesssim \mu_q / \sqrt{\sigma} \lesssim 1.5$, while m_M is not increasing. Further, Figure 3 shows that for $\mu_q / \sqrt{\sigma} \gtrsim 3.4$ the values of both \tilde{m}_M and m_M are smaller than their values at lower μ_q . Thus, we find an indication that the magnetic screening length is increasing at large chemical potential in opposite to the electric screening length and in agreement with perturbation theory. No similar decreasing of m_M was observed in the high temperature QCD or high temperature gluodynamics. Note, that the range of $\mu_q / \sqrt{\sigma} \gtrsim 3.4$ is roughly corresponding to the range where the spatial string tension σ_s is zero, see Figure 5 in Ref. [26].

Comparing with results of Ref. [34] we note that the fluctuation of m_M around a constant value at smaller values of μ_q was also observed in that paper. At large values of μ_q no decreasing of m_M was found in Ref. [34]. In opposite, the results of Ref. [34] hint to

increasing of m_M at large μ_q .

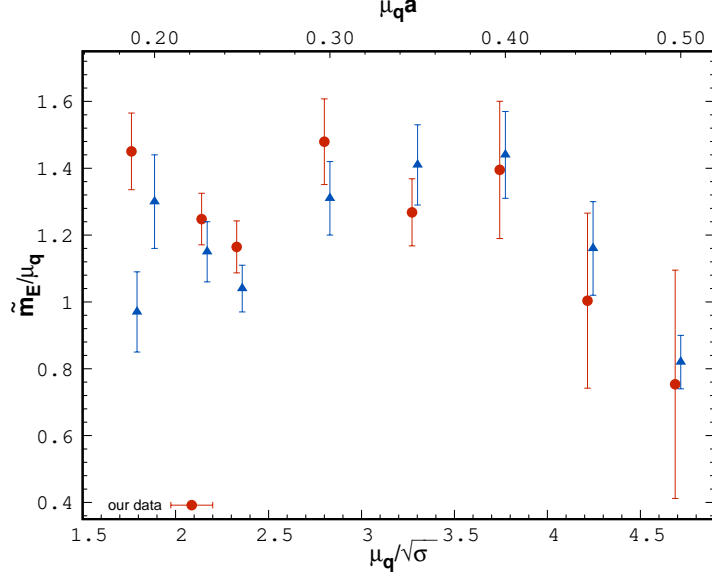


Figure 4. Comparison of the electric screening masses \tilde{m}_E and Debye mass m_D computed in Ref. [27]

In Ref. [27] we computed the Debye screening mass m_D from the singlet quark-anti-quark potential at large distances using the Coulomb gauge. It is expected that m_D should agree with the electric screening mass computed from the gluon propagator. In Figure 4 we compare \tilde{m}_E and m_D . One can see the agreement within a standard deviation at all values of μ_q in the deconfinement phase, i.e. at $\mu_q/\sqrt{\sigma} > 1.9$. Thus, the values of the electric screening mass computed using two different approaches in two different gauges coincide over a wide range of μ_q . We consider this as an important result because it gives some evidence for gauge invariance of the electric screening mass. Note also that the ratio \tilde{m}_E/μ_q is a slowly varying function of μ_q in a qualitative agreement with perturbation theory.

We end this section with a remark on the reason for the differences between our results for the screening masses and results of Ref. [34]. We use a very small value of the lattice spacing in our simulations. This allows us to reach large physical values of μ_q keeping $a\mu_q$ small. In opposite, the values of lattice spacing used in Ref. [34] are at least three times larger and this might cause large lattice artifacts at large μ_q . Another source of the difference in results is the difference in the fermion action discretization used in this paper and in Ref. [34]). Thus results with the Wilson fermions and small lattice spacing are highly needed.

5 $D_L - D_T$ as an indicator of transitions

In the previous two sections we demonstrated that the propagators $D_L(p)$ and $D_T(p)$ become more and more different in the infrared region when the chemical potential is

increasing. At the same time they approach each other at high momenta for fixed μ_q . In this section we study how fast they approach each other with increasing momentum and how the picture changes with increasing μ_q . Similar comparison of these two propagators was undertaken in Ref. [57] in $SU(3)$ gluodynamics at finite temperature where the ratio of the propagators was computed. It was demonstrated that while in the confinement phase $D_L(p)$ is dominating over $D_T(p)$ at all momenta, in the deconfinement phase $D_T(p)$ becomes dominating at high enough momenta.

We will show below that in the theory under study the difference between transverse and longitudinal propagators, $\Delta(p) = D_T(p) - D_L(p)$ has interesting dependence both on momentum and on chemical potential. The important finding is that the soft mode $\Delta(p), p_4 = 0$ which is studied here shows clear exponential dependence on p , which was observed recently also in $SU(2)$ gluodynamics at finite temperature [62].

Our numerical results for $\Delta(p)$ are presented in Figure 5. We show data at $\mu_q/\sqrt{\sigma} =$

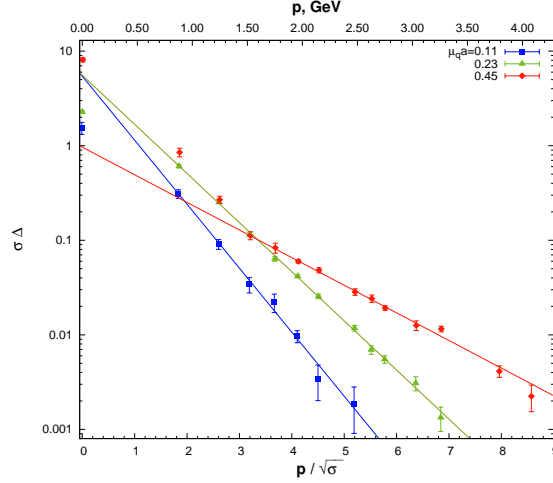


Figure 5. Difference $D_T - D_L$ as functions of p at few values of μ_q .

1.0, 2.2 and 4.2. The exponential decreasing is well established starting from some momentum p_0 depending on μ_q . We found that $p_0 = p_{min}$ for $1.0 \leq \mu_q/\sqrt{\sigma} \leq 3.0$ and $p_0/\sqrt{\sigma} \approx 3.2$ for higher μ_q .

Thus we arrive at a simple fit function to describe the momentum dependence of $\Delta(p)$ at $p > p_0$.

$$\Delta(p) = c \exp(-\nu \cdot p) , \quad (5.1)$$

As a check we compared the fit by function (5.1) with the fit by function

$$\Delta(p) = d \cdot p^v \quad (5.2)$$

motivated by a power-like behavior of both gluon propagators when $p \rightarrow \infty$.

We could not perform fitting for $\mu_q/\sqrt{\sigma} < 0.5$ since $\Delta(p)$ differs from zero at two values of the momentum only. For $0.5 \leq \mu_q/\sqrt{\sigma} \leq 1.0$ $\Delta(p)$ is nonzero for a very few momenta.

For this reason both fit functions work well. At $\mu_q/\sqrt{\sigma} > 1.0$ only the fit function (5.1) works. We show results of our fits for this range of μ_q values in Figure 5.

The dependence of the parameters c and ν on the quark chemical potential is shown in Fig. 6. The exponent ν is linearly decreasing over the range $1.0 \leq \mu_q/\sqrt{\sigma} \leq 4.2$: $\nu(\mu_q)$ can be fitted by the linear function

$$\nu = \nu_0 - \nu_1 \mu_q, \quad (5.3)$$

where $\nu_0 = 1.76(3)/\sqrt{\sigma}$, $\nu_1 = 0.26(1)/\sigma$, $\frac{\chi^2}{N_{d.o.f}} = 2.0$ (p -value = 0.04).

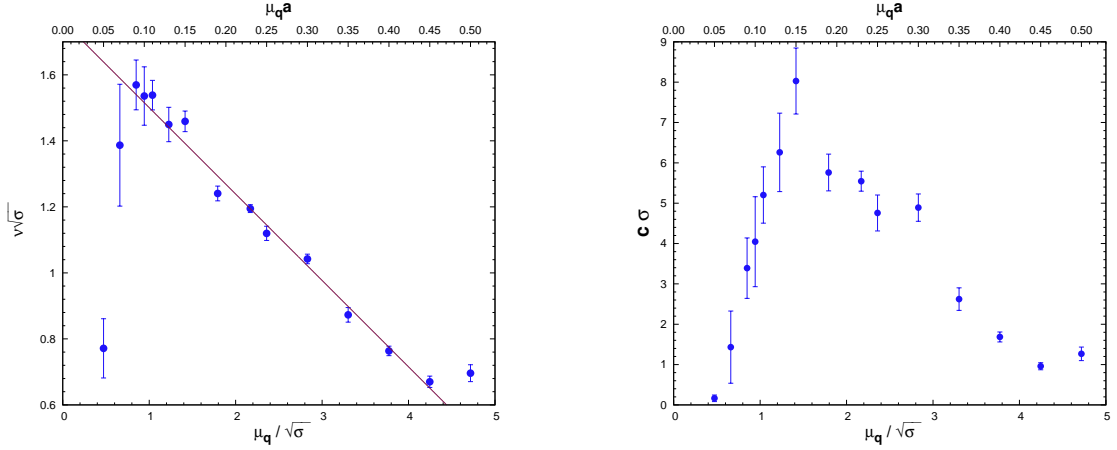


Figure 6. Parameters of the fit (5.1) as functions of μ_q .

6 Conclusions

We presented results of our study of the longitudinal and transverse propagators in the Landau gauge of the QC₂D with $N_f = 2$ lattice staggered quark action at nonzero quark chemical potential. In contrast to earlier studies of the gluon propagators in this theory [30, 34, 38, 39] we employed lattices with very small lattice spacing and were able to reach large physical values for μ_q keeping lattice values of $a\mu_q$ small.

We checked the effects of Gribov copies and found no such effects even in the infrared region. This is different from the results of lattice gluodynamics. There are two reasons for this difference. The Z_2 center symmetry which is a source of the Gribov copies in the gluodynamics with periodic boundary conditions is broken in a theory with the matter field. Another reason is that the physical volume of our lattices is rather small.

Our main observations are as follows. We found that the longitudinal propagator $D_L(p)$ is more and more suppressed in the infrared with increasing μ_q . This is reflected in particular in the increasing of the electric screening mass. Such dependence of $D_L(p)$ on μ_q is analogous to its dependence on temperature at $T > T_c$. In opposite, we found much weaker dependence on μ_q for the transverse propagator $D_T(p)$ with indication of the infrared enhancement at large μ_q .

We considered two definitions of the screening mass. The definition eq. (4.1) is widely used though it has some drawbacks, in particular it depends on renormalization. The other definition eq. (4.3) is renormgroup invariant. We found that both electric masses increase with μ_q and their ratio is a constant factor. A similar relation between the magnetic masses \tilde{m}_M and m_M is not ruled out although our results for \tilde{m}_M have rather large statistical errors.

It is encouraging that our value $\tilde{m}_E/\sqrt{\sigma} = 1.50(4)$ obtained at $\mu_q = 0$ is in a good agreement with respective values found in $SU(2)$ [59] and $SU(3)$ [56] lattice gluodynamics.

Another important result concerning the electric screening mass is a very good agreement between \tilde{m}_E and the Debye screening mass m_D determined from the singlet quark-anti-quark potential at large distances, see Figure 4. This result indicates gauge invariance of the electric screening mass (4.3).

For the magnetic screening masses we found that they show only a weak dependence on μ_q at $\mu_q \lesssim 2.2\sqrt{\sigma}$ with clearly lower values at $\mu_q \gtrsim 3.4\sqrt{\sigma}$. As we know from our previous study [26] this is the range where the spatial string tension becomes zero. This decreasing of the magnetic screening mass is also in agreement with disappearance of the magnetic field screening at extremely large quark chemical potential predicted in [45].

Both increasing of the electric screening mass and decreasing of the magnetic screening mass at large quark densities were not observed before in simulations with Wilson fermions on lattices with coarse lattice spacing [30, 34, 38, 39].

We also studied the difference $\Delta(p) = D_L(p) - D_T(p)$ and found that it decreases exponentially with momentum at large p . The respective exponent is decreasing linearly with μ_q thus indicating that asymmetry between the propagators survives for higher momenta with increasing μ_q .

Acknowledgments

The work was completed due to support of the Russian Foundation for Basic Research via grant 18-02-40130 mega. V. V. B. acknowledges the support from the BASIS foundation. A. A. N. acknowledges the support from STFC via grant ST/P00055X/1. The authors are thankful to Andrey Kotov for participation in the project at the earlier stage and to Jon-Ivar Skullerud and Etsuko Ito for useful discussions.

The research is carried out using the Central Linux Cluster of the NRC "Kurchatov Institute" - IHEP, the equipment of the shared research facilities of HPC computing resources at Lomonosov Moscow State University, the Linux Cluster of the NRC "Kurchatov Institute" - ITEP (Moscow). In addition, we used computer resources of the federal collective usage center Complex for Simulation and Data Processing for Mega-science Facilities at NRC Kurchatov Institute, <http://ckp.nrcki.ru/>.

References

- [1] S. Muroya, A. Nakamura, C. Nonaka, and T. Takaishi, Prog. Theor. Phys. **110**, 615 (2003), [hep-lat/0306031](https://arxiv.org/abs/hep-lat/0306031).

- [2] J. B. Kogut, M. A. Stephanov, D. Toublan, J. J. M. Verbaarschot, and A. Zhitnitsky, Nucl. Phys. **B582**, 477 (2000), [hep-ph/0001171](#).
- [3] D. T. Son and M. A. Stephanov, Phys. Rev. Lett. **86**, 592 (2001), [hep-ph/0005225](#).
- [4] J. B. Kogut and D. K. Sinclair, Phys. Rev. **D66**, 034505 (2002), [hep-lat/0202028](#).
- [5] B. B. Brandt, G. Endrodi, and S. Schmalzbauer, Phys. Rev. **D97**, 054514 (2018), [1712.08190](#).
- [6] L. He and P. Zhuang, Phys. Lett. **B615**, 93 (2005), [hep-ph/0501024](#).
- [7] T. G. Khunjua, K. G. Klimenko, and R. N. Zhokhov, JHEP **06**, 006 (2019), [1901.02855](#).
- [8] T. G. Khunjua, K. G. Klimenko, and R. N. Zhokhov, Phys. Rev. **D97**, 054036 (2018), [1710.09706](#).
- [9] K. Splittorff, D. Toublan, and J. J. M. Verbaarschot, Nucl. Phys. **B620**, 290 (2002), [hep-ph/0108040](#).
- [10] T. Kanazawa, T. Wettig, and N. Yamamoto, JHEP **08**, 003 (2009), [0906.3579](#).
- [11] T. Brauner, K. Fukushima, and Y. Hidaka, Phys. Rev. **D80**, 074035 (2009), [Erratum: Phys. Rev. **D81**, 119904(2010)], [0907.4905](#).
- [12] G.-f. Sun, L. He, and P. Zhuang, Phys. Rev. **D75**, 096004 (2007), [hep-ph/0703159](#).
- [13] L. He, Phys. Rev. **D82**, 096003 (2010), [1007.1920](#).
- [14] N. Strodthoff, B.-J. Schaefer, and L. von Smekal, Phys. Rev. **D85**, 074007 (2012), [1112.5401](#).
- [15] N. Strodthoff and L. von Smekal, Phys. Lett. **B731**, 350 (2014), [1306.2897](#).
- [16] B. Vanderheyden and A. D. Jackson, Phys. Rev. **D64**, 074016 (2001), [hep-ph/0102064](#).
- [17] T. Kanazawa, T. Wettig, and N. Yamamoto, JHEP **12**, 007 (2011), [1110.5858](#).
- [18] R. Contant and M. Q. Huber, Phys. Rev. **D101**, 014016 (2020), [1909.12796](#).
- [19] T. Kojo and G. Baym, Phys. Rev. **D89**, 125008 (2014), [1404.1346](#).
- [20] D. Suenaga and T. Kojo, Phys. Rev. **D100**, 076017 (2019), [1905.08751](#).
- [21] S. Hands, J. B. Kogut, M.-P. Lombardo, and S. E. Morrison, Nucl. Phys. **B558**, 327 (1999), [hep-lat/9902034](#).
- [22] J. B. Kogut, D. Toublan, and D. K. Sinclair, Phys. Lett. **B514**, 77 (2001), [hep-lat/0104010](#).
- [23] J. B. Kogut, D. K. Sinclair, S. J. Hands, and S. E. Morrison, Phys. Rev. **D64**, 094505 (2001), [hep-lat/0105026](#).
- [24] J. B. Kogut, D. Toublan, and D. K. Sinclair, Nucl. Phys. **B642**, 181 (2002), [hep-lat/0205019](#).
- [25] V. V. Braguta, E. M. Ilgenfritz, A. Yu. Kotov, A. V. Molochkov, and A. A. Nikolaev, Phys. Rev. **D94**, 114510 (2016), [1605.04090](#).
- [26] V. G. Bornyakov, V. V. Braguta, E. M. Ilgenfritz, A. Yu. Kotov, A. V. Molochkov, and A. A. Nikolaev, JHEP **03**, 161 (2018), [1711.01869](#).
- [27] N. Yu. Astrakhantsev, V. G. Bornyakov, V. V. Braguta, E. M. Ilgenfritz, A. Yu. Kotov, A. A. Nikolaev, and A. Rothkopf, JHEP **05**, 171 (2019), [1808.06466](#).

- [28] J. Wilhelm, L. Holicki, D. Smith, B. Wellegehausen, and L. von Smekal, Phys. Rev. **D100**, 114507 (2019), [1910.04495](#).
- [29] A. Nakamura, Phys. Lett. **149B**, 391 (1984).
- [30] S. Hands, S. Kim, and J.-I. Skullerud, Eur. Phys. J. **C48**, 193 (2006), [hep-lat/0604004](#).
- [31] S. Hands, S. Kim, and J.-I. Skullerud, Phys. Rev. **D81**, 091502 (2010), [1001.1682](#).
- [32] S. Hands, P. Kenny, S. Kim, and J.-I. Skullerud, Eur. Phys. J. **A47**, 60 (2011), [1101.4961](#).
- [33] S. Cotter, P. Giudice, S. Hands, and J.-I. Skullerud, Phys. Rev. **D87**, 034507 (2013), [1210.4496](#).
- [34] T. Boz, O. Hajizadeh, A. Maas, and J.-I. Skullerud, Phys. Rev. **D99**, 074514 (2019), [1812.08517](#).
- [35] K. Iida, E. Itou, and T.-G. Lee, JHEP **01**, 181 (2020), [1910.07872](#).
- [36] T. Boz, P. Giudice, S. Hands, and J.-I. Skullerud (2019), [1912.10975](#).
- [37] V. Bornyakov, A. Kotov, A. Nikolaev, and R. Rogalyov, in *2nd International Workshop on Theory of Hadronic Matter Under Extreme Conditions Dubna, Russia, September 16-19, 2019* (2019), [1912.08529](#).
- [38] T. Boz, S. Cotter, L. Fister, D. Mehta, and J.-I. Skullerud, Eur. Phys. J. **A49**, 87 (2013), [1303.3223](#).
- [39] O. Hajizadeh, T. Boz, A. Maas, and J.-I. Skullerud, EPJ Web Conf. **175**, 07012 (2018), [1710.06013](#).
- [40] P. Weisz, Nucl. Phys. **B212**, 1 (1983).
- [41] A. Bazavov et al., Phys. Rev. **D85**, 054503 (2012), [1111.1710](#).
- [42] J. E. Mandula and M. Ogilvie, Phys. Lett. **B185**, 127 (1987).
- [43] V. G. Bornyakov, V. K. Mitrjushkin, and M. Muller-Preussker, Phys. Rev. **D81**, 054503 (2010), [0912.4475](#).
- [44] J. I. Kapusta and C. Gale, *Finite-temperature field theory: Principles and applications*, Cambridge Monographs on Mathematical Physics (Cambridge University Press, 2011), ISBN 9780521173223, 9780521820820, 9780511222801.
- [45] D. T. Son, Phys. Rev. **D59**, 094019 (1999), [hep-ph/9812287](#).
- [46] D. Dudal, O. Oliveira, and N. Vandersickel, Phys. Rev. **D81**, 074505 (2010), [1002.2374](#).
- [47] A. Cucchieri, D. Dudal, T. Mendes, and N. Vandersickel, Phys. Rev. **D85**, 094513 (2012), [1111.2327](#).
- [48] O. Oliveira and P. J. Silva, Phys. Rev. **D86**, 114513 (2012), [1207.3029](#).
- [49] D. Dudal, O. Oliveira, and P. J. Silva, Annals Phys. **397**, 351 (2018), [1803.02281](#).
- [50] R. Aouane, V. G. Bornyakov, E. M. Ilgenfritz, V. K. Mitrjushkin, M. Muller-Preussker, and A. Sternbeck, Phys. Rev. **D85**, 034501 (2012), [1108.1735](#).
- [51] D. Dudal, J. A. Gracey, S. P. Sorella, N. Vandersickel, and H. Verschelde, Phys. Rev. **D78**, 065047 (2008), [0806.4348](#).
- [52] C. S. Fischer, A. Maas, and J. A. Muller, Eur.Phys.J. **C68**, 165 (2010), [1003.1960](#).
- [53] A. Maas, Phys. Rept. **524**, 203 (2013), [1106.3942](#).

- [54] V. G. Bornyakov and V. K. Mitrjushkin, Int. J. Mod. Phys. **A27**, 1250050 (2012), [1103.0442](#).
- [55] V. G. Bornyakov and V. K. Mitrjushkin, Phys. Rev. **D84**, 094503 (2011), [1011.4790](#).
- [56] O. Oliveira and P. Bicudo, J. Phys. **G38**, 045003 (2011), [1002.4151](#).
- [57] P. J. Silva, O. Oliveira, P. Bicudo, and N. Cardoso, Phys. Rev. **D89**, 074503 (2014), [1310.5629](#).
- [58] S. Ma, *Modern Theory of critical phenomena* (W. A. Benjamin, Advanced Book Program, Minnesota University, 1976).
- [59] K. Langfeld, H. Reinhardt, and J. Gattnar, Nucl. Phys. **B621**, 131 (2002), [hep-ph/0107141](#).
- [60] A. Maas, J. M. Pawłowski, L. von Smekal, and D. Spielmann, Phys. Rev. **D85**, 034037 (2012), [1110.6340](#).
- [61] A. Hasenfratz and F. Knechtli, Phys. Rev. **D64**, 034504 (2001), [hep-lat/0103029](#).
- [62] V. G. Bornyakov and R. Rogalyov (in preparation).

A Fit results

$\mu_q/\sqrt{\sigma}$	M_L/σ	R_L/σ	$\delta_L\sigma$	p-value	χ^2/N_{dof}	Z_L/σ
0.00	3.34(17)	2.12(48)	0.060(8)	0.68	0.67	16.9
0.28	2.90(13)	0.95(25)	0.082(9)	0.65	0.54	12.6
0.47	3.82(17)	0.79(24)	0.076(8)	0.66	0.53	13.2
0.66	3.80(30)	1.91(67)	0.064(13)	0.27	1.30	15.8
0.85	4.45(33)	1.89(61)	0.057(11)	0.46	0.86	17.0
0.94	4.80(71)	3.2(1.6)	0.050(19)	0.04	2.48	19.9
1.04	5.31(36)	2.95(74)	0.049(9)	0.65	0.67	20.0
1.23	8.0(1.2)	7.9(3.5)	0.023(11)	0.17	1.49	37.6
1.42	8.01(49)	5.6(1.2)	0.031(6)	0.95	0.35	29.4
1.79	10.1(1.4)	7.7(2.8)	0.024(10)	0.38	1.08	37.0
2.17	10.0(1.0)	6.4(1.9)	0.028(8)	0.11	1.58	31.8
2.36	12.8(1.1)	10.2(2.9)	0.019(5)	0.56	0.88	44.4
2.83	18.4(2.3)	13.3(3.9)	0.017(6)	0.49	0.95	53.0
3.77	22.6(4.0)	14.5(4.7)	0.022(10)	0.63	0.82	45.8

Table 1. Parameters of the fits of $D_L(p)$ to function (3.2).

$\mu_q/\sqrt{\sigma}$	M_T/σ	R_T/σ	$\delta_T\sigma$	p -value	χ^2/N_{dof}	Z_T/σ
0.00	3.26(26)	2.93(79)	0.044(9)	0.05	1.94	21.5
0.28	3.09(21)	2.49(60)	0.052(8)	0.00	3.09	19.1
0.47	3.11(14)	2.45(39)	0.052(6)	0.37	1.08	19.0
0.66	3.32(20)	2.52(54)	0.052(8)	0.24	1.29	19.0
0.85	2.91(11)	1.92(30)	0.056(5)	0.51	0.90	17.6
0.94	2.57(15)	1.80(41)	0.067(8)	0.38	1.07	15.6
1.04	2.78(15)	1.26(35)	0.068(8)	0.12	1.58	15.0
1.23	2.66(13)	0.92(26)	0.076(8)	0.14	1.53	13.6
1.42	2.70(17)	0.67(33)	0.070(9)	0.05	1.91	14.4
1.79	3.39(11)	2.40(31)	0.032(3)	0.50	0.92	26.3
2.17	3.86(19)	3.14(59)	0.024(4)	0.08	1.75	32.1
2.36	3.51(19)	3.44(66)	0.024(4)	0.53	0.88	32.9
2.83	3.26(17)	1.68(47)	0.032(4)	0.37	1.09	26.7

Table 2. Parameters of the fit of $D_T(p)$ to function (3.2).